Neutral axis depth and moment redistribution in FRP and steel reinforced concrete continuous beams

Tiejiong Lou, Sergio M.R. Lopes, Adelino V. Lopes

PII: S1359-8368(14)00500-9
DOI: http://dx.doi.org/10.1016/j.compositesb.2014.10.044
Reference: JCOMB 3259

To appear in: *Composites: Part B*

Received Date: 25 August 2014
Revised Date: 5 October 2014
Accepted Date: 27 October 2014

Please cite this article as: Lou, T., Lopes, S.M.R., Lopes, A.V., Neutral axis depth and moment redistribution in FRP and steel reinforced concrete continuous beams, *Composites: Part B* (2014), doi: http://dx.doi.org/10.1016/j.compositesb.2014.10.044

Neutral axis depth and moment redistribution in FRP and steel reinforced concrete continuous beams

Tiejiong Lou[*1], Sergio M. R. Lopes[1], Adelino V. Lopes[2]

1. CEMUC, Department of Civil Engineering, University of Coimbra, Coimbra 3030-788, Portugal
2. Department of Civil Engineering, University of Coimbra, Coimbra 3030-788, Portugal

Abstract: The neutral axis depth is considered the best parameter for quantifying the moment redistribution in continuous concrete beams, as exemplified in various design codes worldwide. It is therefore important to well understand the variation of neutral axis depth against moment redistribution. This paper describes a theoretical investigation into the neutral axis depth and moment redistribution in concrete beams reinforced with fibre reinforced polymer (FRP) and steel bars. A finite element model has been developed. The model predictions are in favourable agreement with experimental results. Three types of reinforcement are considered, namely, glass fibre, carbon fibre and steel. Various levels of reinforcement ratio are used for a parametric evaluation. The results indicate that FRP reinforced concrete continuous beams exhibit significantly different response characteristics regarding the moment redistribution and variation of neutral axis depth from those of steel reinforced ones. In addition, it is found that the code recommendations are generally unsafe for calculating the permissible moment redistribution in FRP reinforced concrete beams, but the neglect of redistribution in such beams may be overconservative.

Keywords: A. Carbon fibre; A. Glass fibre; C. Numerical analysis

* Corresponding author. Tel.: +351 239797253. Email: loutiejiong@dec.uc.pt.

1. Introduction

The bending moments in a continuous beam would be redistributed when any of the constituent materials enters into its inelastic range. The ability of a continuous reinforced concrete beam to redistribute moments is highly dependent on the rotational capacity of critical sections [1,2]. In accordance with various codes adopted worldwide, a linear analysis with permissible redistribution of moments can be used by designers to exploit the ductility of reinforced concrete elements. In general, for practical purposes, very few parameters can be considered in code equations for calculating the amount of moment redistribution. The neutral axis depth is the most common parameter adopted in design codes worldwide (e.g., the Canadian [3], European [4] and British [5] codes), since this parameter can well reflect the plastic rotation capacity of a reinforced concrete section. Therefore, a good understanding of the variation of neutral axis depth against moment redistribution is essential for rational design of continuous reinforced concrete beams.

The employment of fibre reinforced polymer (FRP) for reinforcing concrete elements has become popular owing to its attractive advantages such as high strength, excellent corrosion resistance and low weight [6]. In comparison with conventional steel reinforcement, FRP reinforcement has generally a lower axial stiffness, hence causing larger member deformations. In addition, differently from steel reinforcement with obvious ductile characteristics, FRP reinforcement displays linear-elastic behaviour up to its rupture without yielding, hence giving rise to concerns about the rotational and moment redistribution capacities of FRP reinforced concrete members.

Over past years, extensive theoretical and experimental research has been performed to examine the behaviour of simply-supported FRP reinforced concrete members, in particular, the deflection behaviour and flexural ductility [7-11]. Some researchers have devoted their works to continuous FRP reinforced concrete members. References [12] and [13] presented a set of experimental investigations on flexural behaviour of continuous concrete beams reinforced with GFRP and CFRP bars. El-Mogy et al. [14] tested four two-span continuous specimens, including two GFRP, one CFRP and one steel reinforced concrete beams. Santos et al. [15] conducted an experimental and numerical study of ductility and moment redistribution in continuous GFRP reinforced concrete T-shaped beams. Kara and Ashour [16] assessed redistribution of moments in FRP reinforced concrete beams by comparing the actual moments at ultimate with the corresponding elastic values. More recently, Mahroug et al. [17,18] reported test results of a series of BFRP and CFRP reinforced concrete continuous slabs.

The above literature review indicates that only few contributions are currently available for understanding the behaviour of continuous concrete members reinforced with FRP bars. In particular, the behaviour regarding the moment redistribution and variation of neutral axis depth has not yet been fully understood. This paper presents a numerical investigation on the moment redistribution, as well as the variation of the neutral axis depth, in two-span continuous FRP and steel reinforced concrete beams. Various reinforcement ratios are used. The results of FRP reinforced concrete beams are compared with those of steel ones. A comparative study is also performed on

several design codes where the neutral axis depth is adopted in the calculation of the permissible moment redistribution.

2. Nonlinear model

2.1. Material models

The stress-strain relationship for concrete in uniaxial compression is modelled using a curve recommended in Eurocode 2 [4], as shown in Fig. 1(a); the curve equation is expressed as follows:

$$\frac{\sigma_c}{f_{cm}} = \frac{k\eta - \eta^2}{1 + (k-2)\eta} \tag{1}$$

where $\eta = \varepsilon_c / \varepsilon_{c0}$; σ_c and ε_c are the concrete stress and strain, respectively; $f_{cm} = f_{ck} + 8$, in MPa; f_{ck} is the concrete cylinder compressive strength, in MPa; $\varepsilon_{c0}(‰) = 0.7 f_{cm}^{0.31}$; $k = 1.05 E_c \varepsilon_{c0} / f_{cm}$; and $E_c = 22(f_{cm}/10)^{0.3}$, in GPa. The concrete is assumed to be crushed when its strain reaches the specified ultimate compressive strain. In order to facilitate the numerical modelling, the present analysis assumes that the concrete in compression is linear elastic at initial loading until the elastic stress and strain meet the curve equation indicated by Eq. (1). The concrete in tension is assumed to be linear elastic prior to cracking, followed by linear tension-stiffening behaviour as shown in Fig. 1(b).

The FRP reinforcement is linear elastic up to rupture as shown in Fig. 1(c). The stress-strain behaviour for steel reinforcement in both tension and compression is simulated using a bilinear elastic-hardening law as shown in Fig. 1(d); the modulus for the strain-hardening portion is taken as 1.5% of the steel modulus of elasticity.

2.2. Numerical method

The present study is carried out by using a numerical method which has been developed to simulate the inelastic response of continuous reinforced concrete beams over the complete loading process up to failure [19]. The analysis assumes that a plane section remains plane after deformations, that the reinforcement perfectly bonds with the surrounding concrete and that the geometric nonlinearity is negligible. It should be noted that bond of FRP reinforcement is less effective than that of traditional steel reinforcement. The bond-slip effect for FRP reinforcement may have some influence on the ultimate load and rotation capacity. A more accurate analysis of FRP-reinforced beams should be based on a reasonable bond-slip law for FRP reinforcement [20,21]. For the present study, however, the approximation of perfect bond between FRP reinforcement and concrete is acceptable, since the development of both the neutral axis depth and moment redistribution for FRP-reinforced concrete beams tends to stabilize after reaching a level far below the ultimate load and rotation capacity, as will be indicated later. The proposed numerical method is based on the moment versus curvature relationship pre-generated through the analysis of cross sections. For establishing the moment-curvature relationship of a cross section, the section is divided into concrete and reinforcement layers to include different material properties across the depth of the section. The complete moment-curvature relationship is generated by incrementally varying the prescribed curvature starting from zero and by considering strain compatibility and force equilibriums. The failure of the section is assumed to take place when the compressive concrete or tensile

reinforcement attains its ultimate strain. The typical moment-curvature diagrams for FRP and steel reinforced concrete sections are shown schematically in Fig. 2(a) and (b), respectively. Over the entire loading range, the diagram for the FRP reinforced concrete section consists of two branches with transition due to concrete cracking, while the diagram for the steel reinforced concrete section is composed of three different portions with two turning points caused by concrete cracking and steel yielding, respectively. In the case of unloading, the analysis assumes that the moment decreases linearly with the curvature, with a slope equal to the elastic bending stiffness, as shown in Fig. 2.

The finite element (FE) method is developed utilizing the Timoshenko beam theory, which assumes that a plane section, normal to the centroidal axis before bending, remains plane but is no longer normal to the centroidal axis after bending due to the effects of shear deformations. The beam is divided into a number of two-node beam elements. Each node has two degrees of freedom: transverse displacement w and rotation θ. The transverse displacement and rotation within each element are approximated by linear interpolation. The element nodal displacement vector can be written as $\boldsymbol{u}^e = \{w_1, \theta_1, w_2, \theta_2\}^T$, and denote by $\boldsymbol{P}^e$ the nodal load vector corresponding to $\boldsymbol{u}^e$. By applying the principle of virtual work, the following equilibrium equations can be determined for a single element [19]:

$$\boldsymbol{P}^e = (\boldsymbol{K}_b^e + \boldsymbol{K}_s^e)\boldsymbol{u}^e \tag{2}$$

$$\boldsymbol{K}_b^e = \frac{EI}{l}\begin{bmatrix} 0 & 0 & 0 & 0 \\ 0 & 1 & 0 & -1 \\ 0 & 0 & 0 & 0 \\ 0 & -1 & 0 & 1 \end{bmatrix} \tag{3a}$$

$$\boldsymbol{K}_s^e = \frac{GA}{kl}\begin{bmatrix} 1 & l/2 & -1 & l/2 \\ l/2 & l^2/4 & -l/2 & l^2/4 \\ -1 & -l/2 & 1 & -l/2 \\ l/2 & l^2/4 & -l/2 & l^2/4 \end{bmatrix} \tag{3b}$$

where $\boldsymbol{K}_b^e$ represents the bending stiffness matrix and $\boldsymbol{K}_s^e$ represents the shear stiffness matrix, evaluated using the one-point Gauss quadrature rule; EI is the bending stiffness which is obtained from the pre-generated moment-curvature relationship; GA is the shear stiffness; k is the shear correction factor, taken as 1.2 for a rectangular section; l is the length of the beam element.

The structure equilibrium equations are assembled in the global coordinate system from the contributions of all the elements. A load or displacement control incremental method in combination with the Newton-Raphson iterative scheme is employed to solve the nonlinear equilibrium equations. The iterative scheme for each increment can be summarized as follows: (1) form the element stiffness matrices and assemble them into the total stiffness matrix for the structure; (2) solve equilibrium equations for current displacement increments, and add these increments to the previous nodal displacements to obtain the current nodal displacements; (3) determine the element curvature and shear strain using the strain-displacement equations in the local coordinate system; (4) determine the bending moment and update the bending stiffness based on the pre-generated moment-curvature relationship, and compute the shear force from the shear strain; (5) determine the element end forces and then

assemble them into the internal resisting forces; (6) determine the unbalanced loads, and repeat the above steps until convergence is achieved. During the solution process, when one of the elements reaches its ultimate curvature capacity, the beam fails and the analysis is therefore finished. More details about the numerical procedure of the proposed analysis can be seen in Lou et al. [19].

2.3. Comparison with experimental results

In order to validate the proposed nonlinear model, five of the continuous reinforced concrete beams tested in Coimbra have been analysed. These beams were V1-0.7, V1-1.4, V1-2.9, V1-3.8 and V1-5.0. All the beams had a rectangular section (120×220 mm) and the same length of 6.0 m, with two equal spans to which two concentrated loads were applied. The main variable for the beams was the tensile reinforcement area over the centre support region: 157 (V1-0.7), 314 (V1-1.4), 628 (V1-2.9), 804 (V1-3.8) and 1030 mm^2 (V1-5.0). More details about the specimens can be found elsewhere [22,23]. Fig. 3 shows a comparison between the computational and experimental results regarding the development of centre and end support reactions with the applied load for the test beams. It can be observed that the proposed analysis reproduces the experimental results very well throughout the loading process up to failure.

3. Numerical study

A two-span continuous reinforced concrete rectangular beam, as shown Fig. 4, is used for the present investigation. Each span is subjected to a concentrated load at

midspan. Three types of reinforcement are selected, namely, GFRP, CFRP and steel reinforcement. The ultimate strength, ultimate strain and elastic modulus for GFRP are 620 MPa, 1.49% and 41.6 GPa, respectively; those for CFRP are 1450 MPa, 1.09% and 133 GPa, respectively; the yield strength and elastic modulus for steel are 530 MPa and 200 GPa, respectively. The amounts of reinforcement are as follows: A_{r2} = 1000–5000 mm^2 (ρ_{r2} = 0.61%–3.03%); A_{r2}/A_{r1} (or ρ_{r2}/ρ_{r1}) = 2/3; A_{r3} = 600 mm^2 (ρ_{r3} = 0.36%), where A_{r1} (ρ_{r1}), A_{r2} (ρ_{r2}) and A_{r3} (ρ_{r3}) are the tensile reinforcement areas (ratios) over the positive and negative moment regions and the compressive reinforcement area (ratio), respectively. The concrete strength f_{ck} is 60 MPa.

3.1. Neutral axis depth

Fig. 5 illustrates the development of neutral axis depths at the midspan and centre support with the applied load for the beams with different types of reinforcement (ρ_{r2} = 1.82%). The position of the neutral axis at a section prior to cracking remains unchanged, locating at the centroidal axis of the transformed section (the reinforcement area is transformed into the equivalent area of concrete). Since the amount of tensile reinforcement at midspan is higher than that at the centre support, the initial neutral axis depth at midspan is higher than that at the centre support. In addition, depending on the level of the modulus of elasticity, GFRP reinforcement develops the lowest initial neutral axis depth at midspan or centre support, while steel reinforcement registers the highest one. After a section is loaded to be cracked, the neutral axis depth at the section decreases rapidly at first and tends to stabilize with the stabilization of the crack evolution. For FRP reinforcement, the stabilizing

behaviour continues up to the ultimate failure of the beams. For steel reinforcement, on the other hand, the yielding of tensile steel in the section leads to a quick decrease in the neutral axis depth. This phenomenon is particularly obvious for the midspan section, attributed to that this section is heavily reinforced and also to that this section yields behind the centre support section.

The neutral axis depth versus curvature behaviour for the beams is shown in Fig. 6. Before cracking, the neutral axis does not move and the variation of the curvature is negligible. After cracking, the movement of the neutral axis with increasing curvature is very fast in the beginning and gradually slows down. For steel reinforcement, a quick movement resumes after yielding of the reinforcement. The movement of the neutral axis depth for different types of reinforcement depends on the elastic modulus and ductile characteristic of the reinforcement. When compared to FRP reinforcement, steel reinforcement mobilizes a slower movement of the neutral axis depth before steel yielding but registers a much faster variation after steel yielding.

Fig. 7 shows the variation of the normalized neutral axis depth, c_u/d (c_u is the neutral axis depth at ultimate and d is the effective depth of a section), with the reinforcement ratio for midspan and centre support sections of FRP and steel reinforced concrete beams. It is seen that, for a given type of reinforcement, the value of c_u/d increases with the increase of the reinforcement ratio. Also, the midspan section registers higher value of c_u/d than the centre support section, while the difference between the c_u/d values for the midspan and centre support tends to enlarge as the reinforcement ratio increases, particularly notable for steel reinforcement. Due

to higher axial stiffness, CFRP reinforcement mobilizes higher value of c_u/d for a critical section when compared to GFRP reinforcement, particularly at a high reinforcement ratio. At the lowest reinforcement ratio of 0.61%, the difference between the c_u/d values for steel and GFRP reinforcement is insignificant while steel reinforcement mobilizes obviously lower value of c_u/d than CFRP reinforcement. As the reinforcement ratio increases, the increase in neutral axis depth for steel reinforcement tends to be faster than that for FRP reinforcement, especially at the midspan section.

3.2. Moment redistribution

Fig. 8(a), (b) and (c) show the development of applied moments at midspan M_{L1} and centre support M_{L2}, as well as the evolution of the moment ratio M_{L2}/M_{L1}, for GFRP, CFRP and steel reinforced concrete beams (ρ_{r2} = 1.82%), respectively. The applied moment shown in the graphs is contributed by the applied load, not including the moment due to self-weight of the beam. The elastic moment ratio $(M_{L2}/M_{L1})_{ela}$, which is calculated assuming the materials are linear elastic and therefore remains constant during the loading process, is also displayed in the graphs. The values of $(M_{L2}/M_{L1})_{ela}$ for GFRP, CFRP and steel reinforced concrete beams are 1.17, 1.15 and 1.14, respectively. The slight difference between the values is attributed to the different moduli of elasticity for different types of reinforcement. It can be observed in the graphs that, at initial loading, the moments increase linearly with the applied load and, accordingly, the actual moment ratio is equal to the elastic one, indicating that there is no moment redistribution in this elastic stage. When a first crack appears

at the centre support, the moments begin to be redistributed from the centre support towards the midspan, resulting in a faster growth of the midspan moment and correspondingly a slower growth of the centre support moment. As a consequence, the actual moment ratio begins to diminish. After stabilizing of the crack evolution, the development of moments and the value of the moment ratio also stabilize. For FRP reinforcement this phenomenon lasts up to the ultimate failure, as illustrated in Fig. 8(a) and (b). For steel reinforcement, on the other hand, the yielding of the centre support reinforcement causes an accentuation of moment redistribution away from the centre support. As a result, the centre support moment grows much slower while the midspan moment increases much quicker, leading to a quick decrease in the moment ratio, as can be seen in Fig. 8(c).

The redistribution of moments may be quantified by: $\beta = 1 - (M / M_e)$, where β is the degree of moment redistribution; M and M_e are the actual and elastic moments at a certain load level, respectively. Fig. 9 demonstrates the variation of the degree of moment redistribution with the applied load for the beams with different types of reinforcement. For FRP reinforcement, the entire response consists of three different stages with two turning points corresponding to the onset of cracking (at the centre support) and the stabilization of crack development, respectively. In the first stage, the moment redistribution does not yet take place and, therefore, the degree of moment redistribution is equal to zero; in the second stage, the redistribution of moments (positive at the centre support but negative at midspan) quickly increases, with almost a linear manner with the applied load; in the third stage, the degree of moment

redistribution tends to stabilize. For steel reinforcement, on the other hand, the steel yielding (at the centre support) leads to an additional stage, in which the degree of moment redistribution increases very quickly.

Fig. 10 shows the variation of the degree of moment redistribution at ultimate, β_u, with the reinforcement ratio. It is seen that the value of β_u tends to decrease with the increase of the reinforcement ratio, except at low ratios of GFRP reinforcement (ρ_{r2} < 1.21%). At a given reinforcement ratio, GFRP reinforcement generally mobilizes higher redistribution at ultimate than CFRP reinforcement, particularly at high reinforcement ratio levels. Steel reinforcement develops significantly higher redistribution at ultimate than FRP reinforcement, particularly at low reinforcement ratio levels. It should be noted that the contribution of FRP reinforcement to moment redistribution is highly dependent on the structural typology. The moment redistribution behaviour of other typologies of members may be quite different from that of reinforced concrete beams as examined in this study. For example, in externally post-tensioned members, the moment redistribution by FRP tendons can be considerable and comparable to that by steel tendons [24,25].

4. Evaluation of design codes

4.1. Relationship between moment redistribution and neutral axis depth according to code recommendations

In many codes of practice, the moment at a critical section can be calculated by elastic theory with allowable redistribution of moments. Most of the design codes

adopt the normalized neutral axis depth c_u/d to calculate the degree of moment redistribution, including the Canadian [3], European [4] and British [5] codes.

(1) Canadian code

According to the recommendation by Canadian Standards Association [3], the negative moments at supports obtained by an elastic analysis can be increased or reduced by at most ($30–50c_u/d$) percent, with a maximum of 20%.

$$\beta_u \le (30 - 50c_u / d)\% \le 20\% \tag{4}$$

(2) European code

In Europe, Eurocode 2 [4] indicates that a linear elastic analysis with limited moment redistribution may be applicable, without explicit verification of the rotation capacity, to continuous beams or slabs which are predominantly under flexure and have a ratio of the lengths of adjacent spans ranging between 0.5 and 2. The redistribution of moments is determined by

$$\beta_u \le \lambda - 1.25[0.6 + (0.0014 / \varepsilon_u)]c_u / d \tag{5}$$

where λ is a coefficient depending on the concrete strength; the value of λ is 0.56 for normal-strength concrete and 0.46 for high-strength concrete. The maximum redistribution is 30% for high and normal-ductility steel and 20% for low-ductility steel. In this study, the maximum redistribution for FRP reinforcement is considered to be 20%.

(3) British code

The British standard [5] indicates that the redistribution of the moments calculated by an elastic analysis may be carried out provided that the neutral axis depth c_u of the

cross section, where the design ultimate moment is to be reduced, is not higher than (δ–0.4)d, where δ is the ratio of the moment at the section after redistribution to the moment calculated in terms of the theory of elasticity and the minimum of δ is 70%. Accordingly, the degree of moment redistribution is calculated by

$$\beta_u \le (60 - 100 c_u / d)\% \le 30\% \quad (6)$$

4.2. Comparison between numerical and code predictions

Fig. 11 shows the β_u-c_u/d relationships predicted by the FE analysis for the centre support section of FRP and steel reinforced concrete beams as well as the relationships in terms of various codes. It is seen that, according to the numerical analysis, the β_u value decreases as c_u/d increases, except for the GFRP reinforced concrete beam with c_u/d not greater than 0.17. The decrease in the β_u value with increasing c_u/d for steel reinforcement is faster than those for GFRP and CFRP reinforcement, which are almost at the same rate. Also, for the FRP reinforced concrete beams where c_u/d is greater than 0.17, there is an approximately linear relationship between the degree of moment redistribution and the neutral axis depth at ultimate, regardless of the type of FRP reinforcement. At a given level of c_u/d, the β_u value for steel reinforcement is much higher than that for FRP reinforcement, especially at a low c_u/d ratio.

Comparing the β_u-c_u/d curves by numerical and code predictions, it is observed that the British code is nonconservative for all the analysed beams. The Canadian code is conservative for steel reinforcement but nonconservative for FRP reinforcement. For steel reinforcement, the European code is generally conservative

but may be overconservative at high values of c_u/d; for FRP reinforcement, the European code is conservative at high values of c_u/d but nonconservative at low values of c_u/d.

Fig. 12(a), (b) and (c) display a comparison of the β_u values obtained by various codes with the results computed by the FE analysis for the GFRP, CFRP and steel reinforced concrete beams, respectively. As far as the variation of β_u with the reinforcement ratio is concerned, all the codes can satisfactorily reflect the actual trend predicted by the numerical analysis, although the European and British codes exhibit a sharper slope. For GFRP reinforcement, all the codes are nonconservative over the whole range of reinforcement ratio, especially for the British code. For CFRP reinforcement, the Canadian and British codes are nonconservative; the European code is nonconservative for ρ_{r2} lower than about 1.14% but may be overconservative at a high level of reinforcement ratio. For steel reinforcement, the Canadian and European codes are conservative while the British code is nonconservative.

Fig. 13(a), (b) and (c) illustrate the influence of the type of reinforcement on the degree of moment redistribution according to the predictions by the Canadian, European and British codes, respectively. The results obtained by the FE analysis are also included in the graphs for comparison purposes. It is seen that, according to the code predictions, at a given reinforcement ratio GFRP reinforcement generally mobilizes higher redistribution at ultimate than steel reinforcement. However, this is incorrect because, based on the predictions by the FE analysis, the redistribution for

GFRP reinforcement is significantly lower than that for steel reinforcement. It can also be observed that the codes substantially underestimate the actual difference between the degrees of redistribution for CFRP and steel reinforcement. Therefore, the current rules related to moment redistribution, which were initially proposed for steel reinforcement, cannot be simply applied to FRP reinforcement. The current codes are generally unsafe in predicting the redistribution of moment at ultimate in FRP reinforced concrete beams. On the other hand, it may be overconservative if the redistribution of moments in these beams is neglected. For the FRP reinforced concrete beams used in this study, the degrees of redistribution are between a minimum of 8.07% and a maximum of 12.46%. The fit curve equation illustrated in Fig. 11 may be used for calculating the degree of redistribution in FRP reinforced concrete beams.

5. Conclusions

Based on a numerical study conducted on two-span continuous FRP and steel reinforced concrete beams, the following conclusions regarding the neutral axis depth and moment redistribution can be drawn:

(1) For steel reinforced concrete beams, the yielding of reinforcement plays a very important role in the evolution of neutral axis depth and moment redistribution. Due to the lack of reinforcement yielding, FRP reinforced concrete continuous beams exhibit quite different response characteristics compared to steel reinforced ones.

(2) At a low reinforcement ratio, the neutral axis depths at ultimate for GFRP and steel reinforcement are really close, but CFRP reinforcement mobilizes obviously higher neutral axis depth compared to steel reinforcement. As the reinforced ratio increases, the increase in neutral axis depth for steel reinforcement is faster than that for FRP reinforcement.

(3) At a given reinforcement ratio, the moment redistribution at ultimate for steel reinforcement is much higher than that for FRP reinforcement, especially at low reinforcement ratios. Due to lower axial stiffness, GFRP reinforcement tends to mobilize higher redistribution than CFRP reinforcement, particularly obvious at high reinforcement ratios.

(4) In general, the current design codes, initially developed for steel reinforcement, are not safe when used to predict the moment redistribution in FRP reinforced concrete beams. On the other hand, the neglect of moment redistribution in concrete beams reinforced with FRP bars may be overconservative, since the degree of redistribution at ultimate in these beams can reach around 10% according to the results of the present analysis.

Acknowledgements

This research is sponsored by FEDER funds through the programme COMPETE (Programa Operacional Factores de Competitividade) and by national funds through FCT (Fundação para a Ciência e a Tecnologia) under the project PEst-C/EME/UI0285/2013. The work presented in this paper has also been supported

by FCT under Grant No. SFRH/BPD/66453/2009.

References

[1] Scott RH, Whittle RT. Moment redistribution effects in beams. Magazine of Concrete Research 2005; 57(1): 9-20.

[2] Oehlers DJ, Haskett M, Mohamed Ali MS, Griffith MC. Moment redistribution in reinforced concrete beams. Proceedings of the Institute of Civil Engineers – Structures & Buildings 2010; 163 (SB3): 165-176.

[3] Canadian Standards Association (CSA). Design of concrete structures. A23.3-04, Mississauga, Ontario, Canada; 2004.

[4] European Committee for Standardization (CEN). Eurocode 2: Design of concrete structures – Part 1-1: General rules and rules for buildings. EN 1992-1-1, Brussels, Belgium; 2004.

[5] British Standards Institution (BSI). Structural use of Concrete – Part 1: Code of practice for design and construction. BS8110, London, UK; 2007.

[6] Baena M, Torres L, Turon A, Mias C. Analysis of cracking behaviour and tension stiffening in FRP reinforced concrete tensile elements. Composites Part B: Engineering 2013; 45: 1360-1367.

[7] Wang H, Belarbi A. Ductility characteristics of fiber-reinforced-concrete beams reinforced with FRP rebars. Construction and Building Materials 2011; 25: 2391-2401.

[8] Al-Sunna R, Pilakoutas k, Hajirasouliha I, GuadagniniM. Deflection behaviour of

FRP reinforced concrete beams and slabs: an experimental investigation. Composites Part B: Engineering 2012; 43: 2125-2134.

[9] Mias C, Torres L, Turon A, Sharaky IA. Effect of material properties on long-term deflections of GFRP reinforced concrete beams. Construction and Building Materials 2013; 41: 99-108.

[10] Kara IF, Ashour AF, Dundar C. Deflection of concrete structures reinforced with FRP bars. Composites Part B: Engineering 2013; 44: 375-384.

[11] Oehlers DJ, Muhamad R, Mohamed Ali MS. Serviceability flexural ductility of FRP RC beams: a discrete rotation approach. Construction and Building Materials 2013; 49: 974-984.

[12] Habeeb MN, Ashour AF. Flexural behavior of continuous GFRP reinforced concrete beams. ASCE Journal of Composites for Construction 2008; 12(2): 115-124.

[13] Ashour AF, Habeeb MN. Continuous concrete beams reinforced with CFRP bars. Proceedings of the Institution of Civil Engineering – Structures & Buildings 2008; 161(SB6): 349-357.

[14] El-Mogy M, El-Ragaby A, El-Salakawy E. Flexural behavior of continuous FRP-reinforced concrete beams. ASCE Journal of Composites for Construction 2010; 14(6): 669-680.

[15] Santos P, Laranja G, Franca PM, Correia JR. Ductility and moment redistribution capacity of multi-span T-section concrete beams reinforced with GFRP bars. Construction and Building Materials 2013; 49: 949-961.

[16] Kara IF, Ashour AF. Moment redistribution in continuous FRP reinforced concrete beams. Construction and Building Materials 2013; 49: 939-948.

[17] Mahroug MEM, Ashour AF, Lam D. Experimental response and code modelling of continuous concrete slabs reinforced with BFRP bars. Composite Structures 2014; 107: 664-674.

[18] Mahroug MEM, Ashour AF, Lam D. Tests of continuous concrete slabs reinforced with carbon fibre reinforced polymer bars. Composites Part B: Engineering 2014; 66: 348-357.

[19] Lou T, Lopes SMR, Lopes AV. FE modeling of inelastic behavior of reinforced high-strength concrete continuous beams. Structural Engineering and Mechanics 2014; 49(3): 373-393.

[20] Mazaheripour H, Barros J, Sena-Cruz J, Pepe M, Martinelli E. Experimental study on bond performance of GFRP bars in self-compacting steel fiber reinforced concrete. Composite Structures 2013; 95: 202-212.

[21] Pepe M, Mazaheripour H, Barros J, Sena-Cruz J, Martinelli E. Numerical calibration of bond law for GFRP bars embedded in steel fibre-reinforced self-compacting concrete. Composites Part B: Engineering 2013; 50: 403-412.

[22] Carmo RNF. Plastic rotation and moment redistribution in high strength concrete beams. PhD thesis, University of Coimbra, Coimbra, Portugal; 2004. (in Portuguese)

[23] Carmo RNF, Lopes SMR. Available plastic rotation in continuous high-strength concrete beams. Canadian Journal of Civil Engineering 2008; 35(10): 1152-1162.

[24] Lou T, Lopes SMR, Lopes AV. External CFRP tendon members: Secondary reactions and moment redistribution. Composites Part B: Engineering 2014; 57: 250-261.

[25] Lou T, Lopes SMR, Lopes AV. Factors affecting moment redistribution at ultimate in continuous beams prestressed with external CFRP tendons. Composites Part B: Engineering 2014; 66: 136-146.

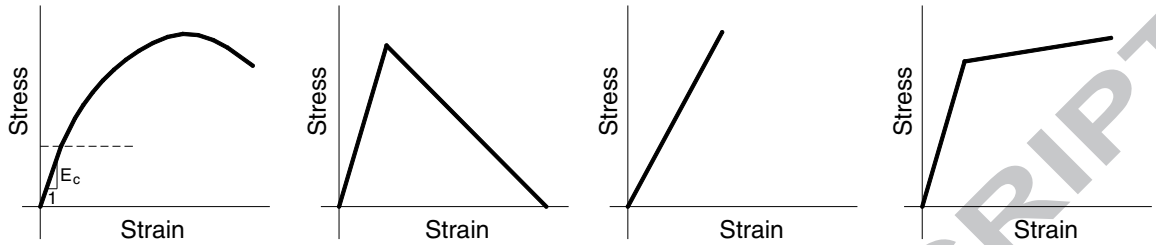

(a) (b) (c) (d)

Fig. 1. Stress-strain diagrams of materials. (a) concrete in compression; (b) concrete in tension; (c) FRP reinforcement; (d) steel reinforcement.

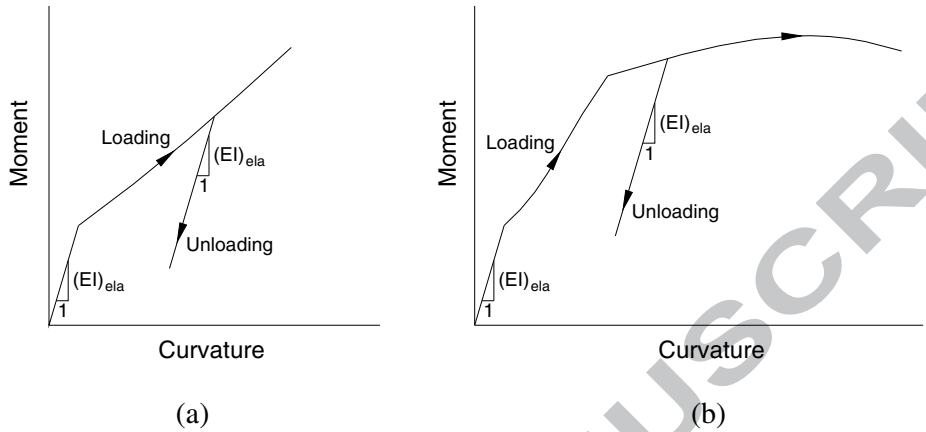

Fig. 2. Schematic moment-curvature diagrams of reinforced concrete sections. (a) FRP reinforced concrete section; (b) steel reinforced concrete section.

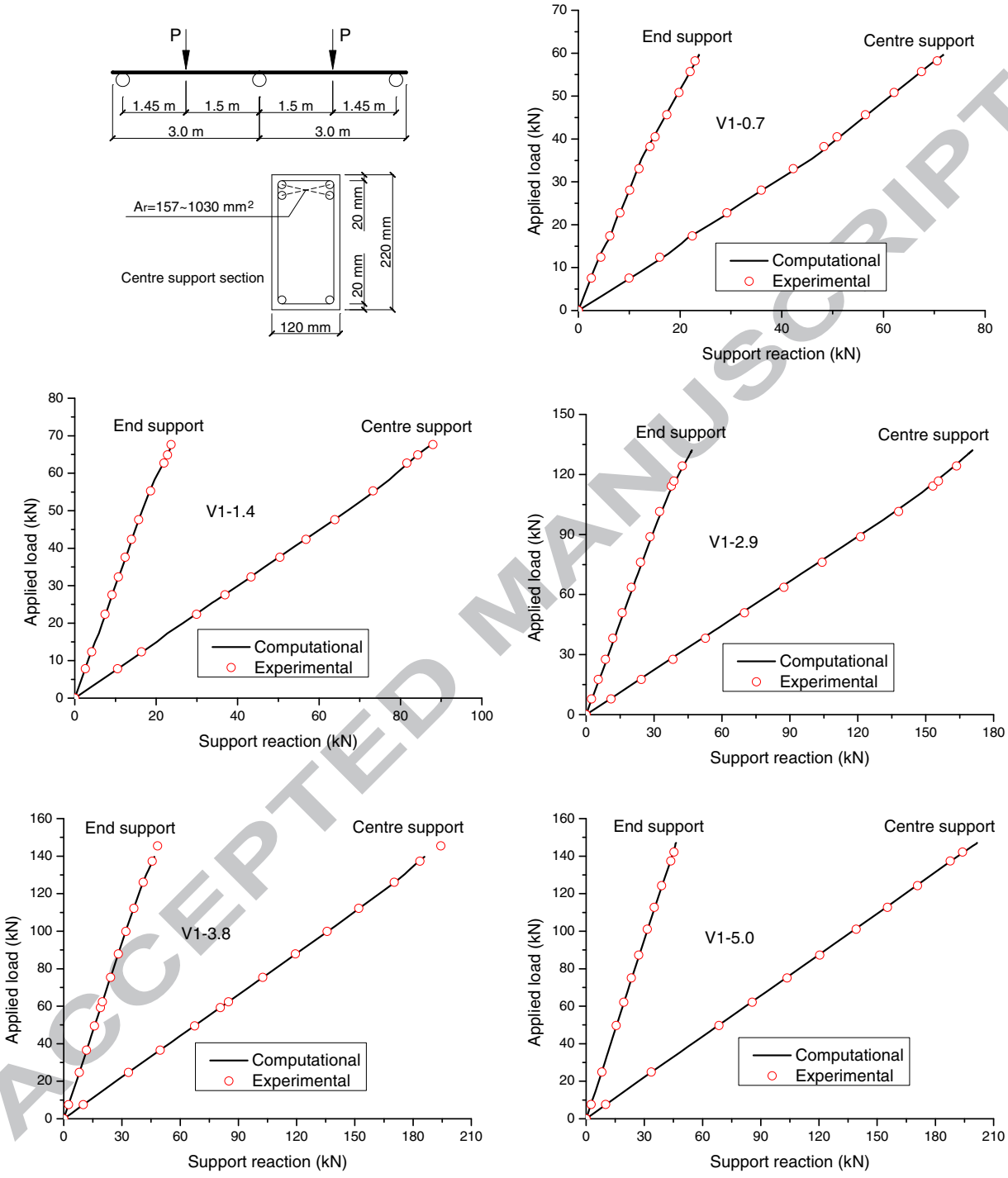

Fig. 3. Comparison between predicted load-reaction responses and experimental ones for test beams.

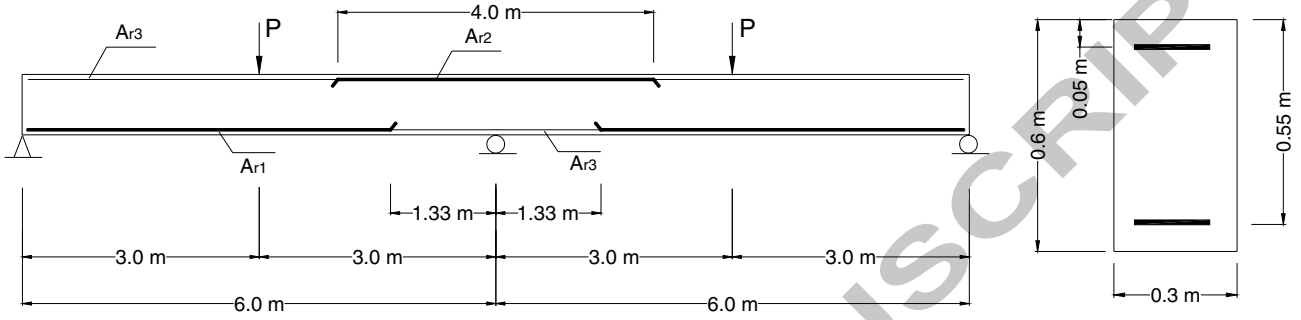

Fig. 4. Details of reinforced concrete beam for numerical evaluation.

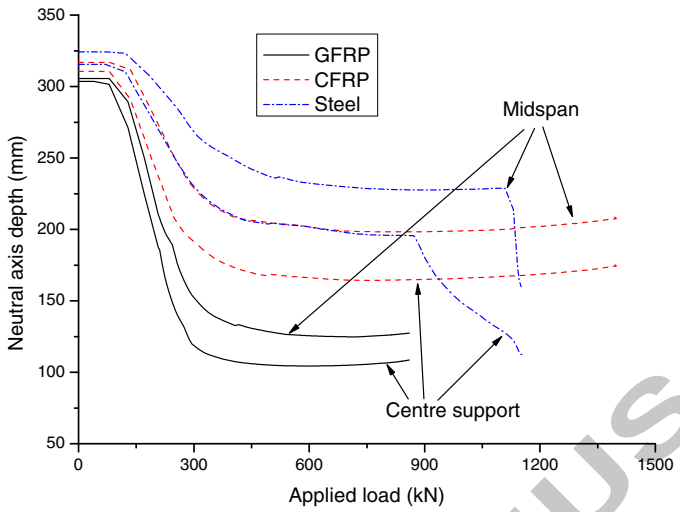

Fig. 5. Development of neutral axis depth with applied load for the beams with different types of reinforcement (ρ_{r2} = 1.82%).

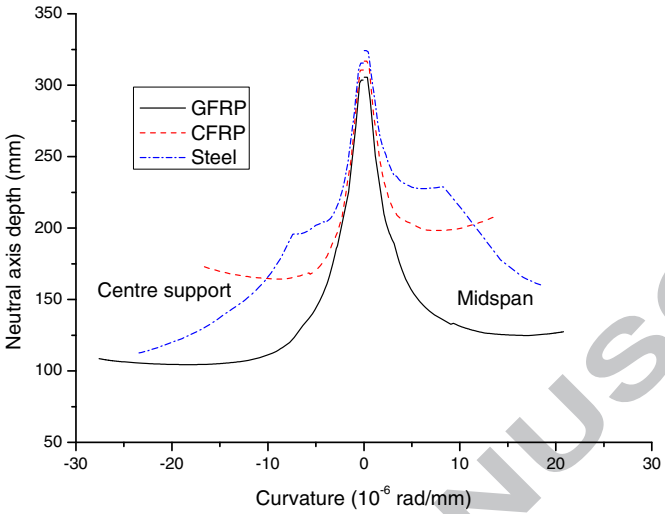

Fig. 6. Development of neutral axis depth with curvature for the beams with different types of reinforcement (ρ_{r2} = 1.82%).

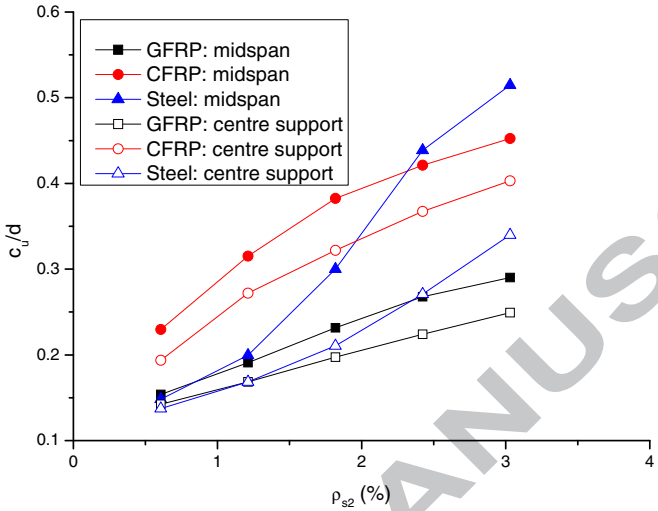

Fig. 7. Variation of neutral axis depth at ultimate with reinforcement ratio.

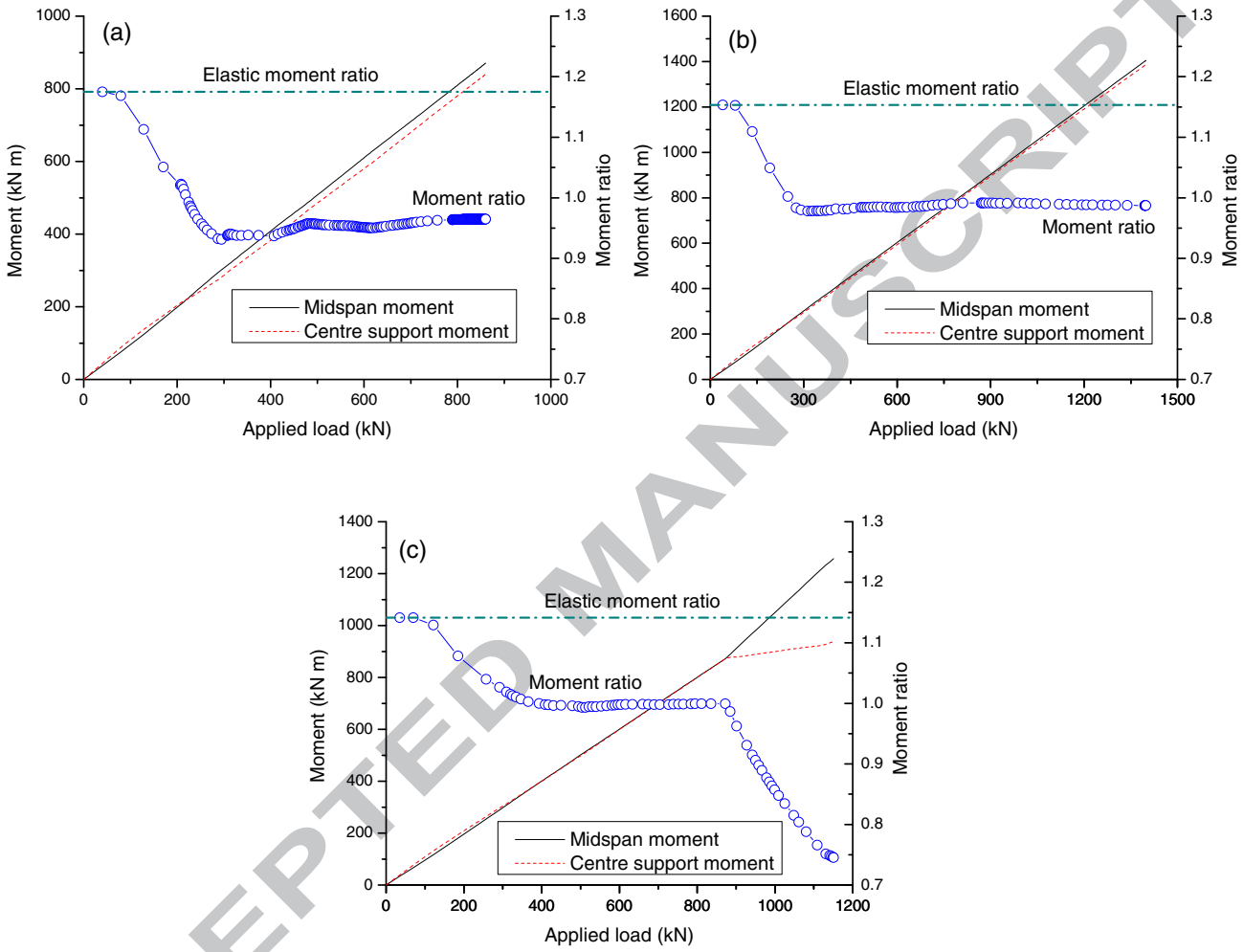

Fig. 8. Development of moment and moment ratio for the beams with different types of reinforcement (ρ_{r2} = 1.82%). (a) GFRP reinforcement; (b) CFRP reinforcement; (c) steel reinforcement.

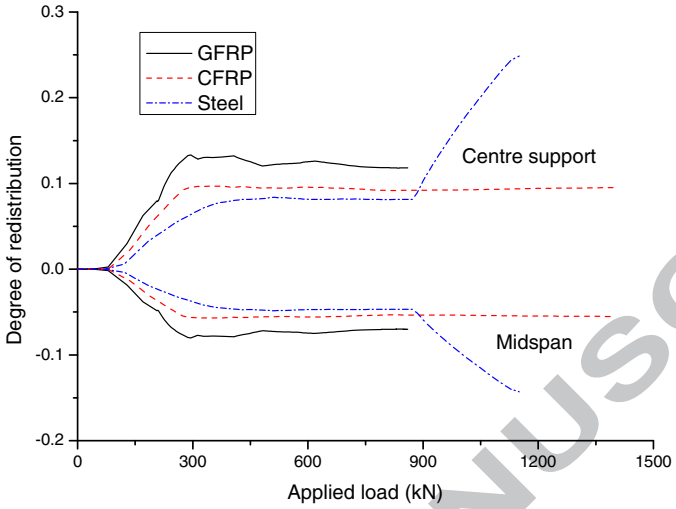

Fig. 9. Development of the degree of redistribution with applied load for the beams with different types of reinforcement (ρ_{r2} = 1.82%).

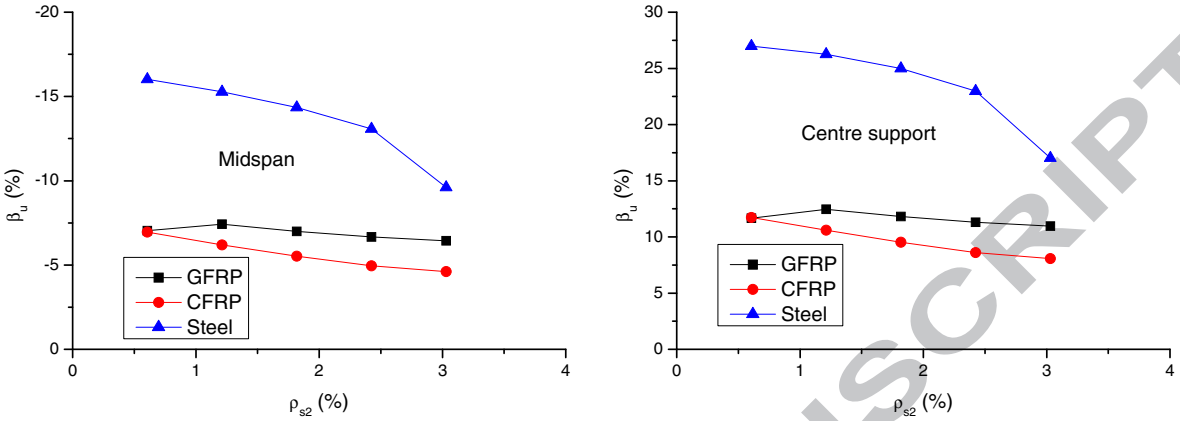

Fig. 10. Variation of the degree of redistribution at ultimate with reinforcement ratio.

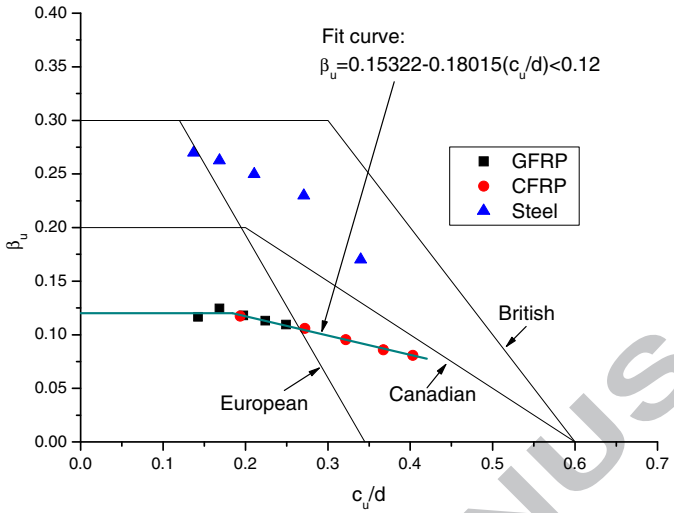

Fig. 11. Relationship between moment redistribution and neutral axis depth at ultimate.

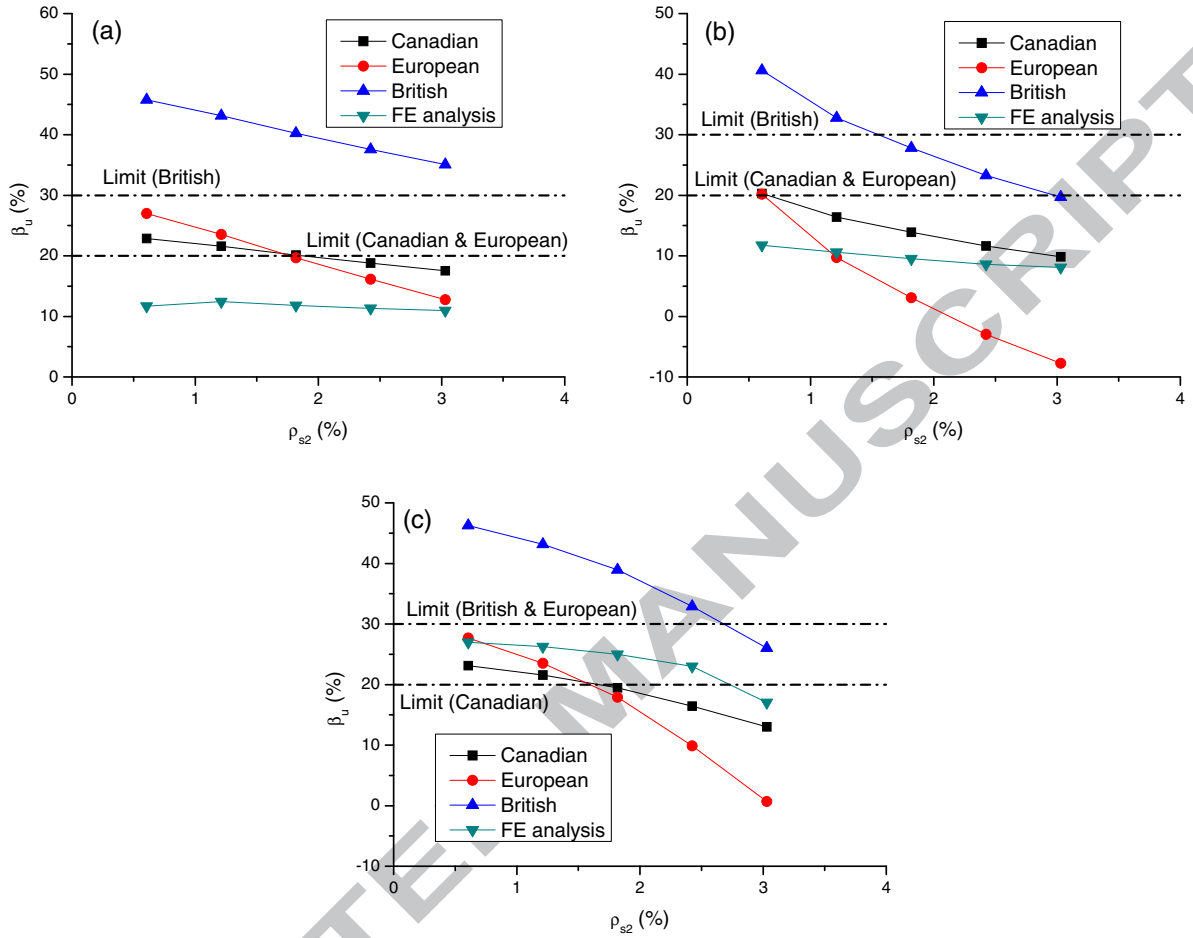

Fig. 12. Comparison between the degrees of redistribution at ultimate obtained by design codes and numerical analysis. (a) GFRP reinforcement; (b) CFRP reinforcement; (c) steel reinforcement.

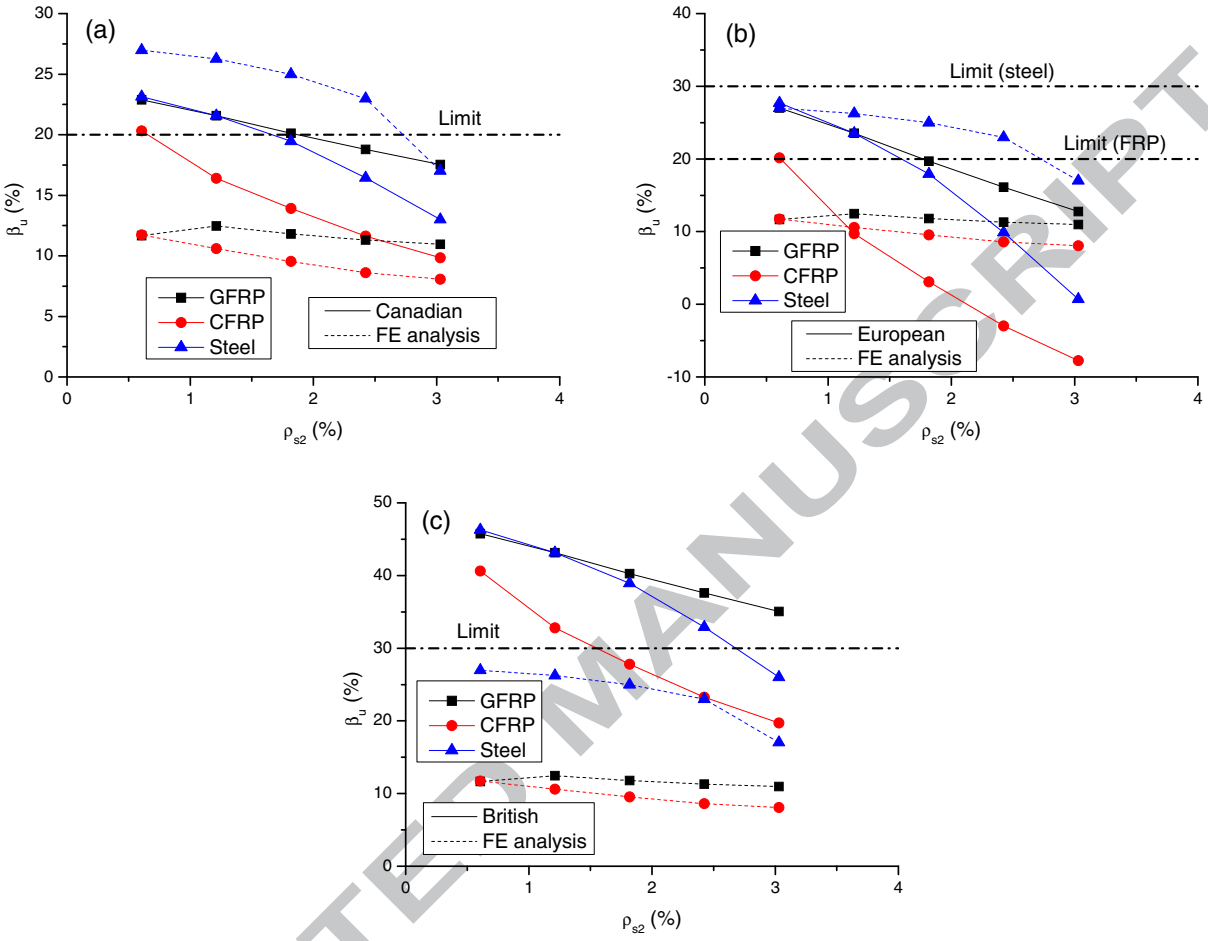

Fig. 13. Effect of reinforcement type on the moment redistribution at ultimate according to design codes. (a) Canadian code; (b) European code; (c) British code.